the methoxybenzenes is the nonadditivity of incremental free energy changes in the trimethoprim series. We have ascribed these differences to the inherent differences between ethyl and hydrogen solvation thermodynamics and flexibility.

Finally, we note that this study paves the way for a detailed examination of "drug design" strategies by thermodynamic simulations, using as a prototypical system the binding of trimethoprim congeners to the enzyme dihydrofolate reductase. The presentation of these results and a discussion of their interpretation are forthcoming.

Spectroscopic Characterization of Lanthanide Octaethylporphyrin Sandwich Complexes. Effects of Strong $\pi\pi$ Interaction

John K. Duchowski and David F. Bocian*

Contribution from the Department of Chemistry, Carnegie Mellon University, Pittsburgh, Pennsylvania 15213. Received September 25, 1989

Abstract: Optical absorption and resonance Raman spectra are reported for the lanthanide sandwich porphyrins, $Eu^{III}(OEP)_2$, $Nd^{III}(OEP)_2$, and $La^{III}(OEP)_2$ (OEP = octaethylporphyrin). These complexes contain a single hole in the porphyrin π system and are electronically similar to the Ce^{IV} sandwich porphyrin cation radical $Ce^{IV}(OEP)_2^+$. Variable-temperature (10–300 K) UV–vis and near-infrared (NIR) spectra are obtained for all four single-hole sandwiches. At high resolution and/or at low temperatures, well-resolved fine structure is observed on the intradimer charge-transfer bands (ca. 1250 nm) of all the complexes. The absorption is dominated by a single Franck–Condon active vibration. This vibration is assigned as a mode, Q_{AB}, which contains a significant amount of multicenter character and modulates interring separation. Vibronic analysis of the NIR band contours reveals that two system origins, separated by 400–700 cm^{-1} (depending on the complex), are present. The progressions built off the lower and higher energy origins exhibit spacings of $\sim$250 and $\sim$315 cm^{-1}, respectively. The existence of two forms which differ in the relative orientation of their ethyl groups is suggested as the source of the double origin in the NIR region. The vibronic analysis indicates that the frequencies of the Q_{AB} modes of either form are $\sim$120 cm^{-1} higher in the ground electronic state than in the charge-transfer excited state. The dimensionless origin shifts, Δ, along Q_{AB} are similar (although not exactly identical) for the two forms and range from 2.6 to 3.0 depending on the complex. These values of Δ correspond to differences in interring separation of $\sim$0.05 Å between the ground and charge-transfer excited states. Collectively, the spectroscopic data indicate that the holes of all the sandwich complexes are delocalized over both rings on the vibrational and electronic time scales and that approximately 1/4 to 1/3 of the intradimer bonding in the ground electronic state can be attributed to $\pi\pi$ interaction.

I. Introduction

Photosynthetic proteins and certain organic conductors share the common feature of closely spaced porphyrinic π systems.[1-5] Strong electronic interactions between molecules within these natural and synthetic aggregates impart unique electron transfer and/or conductivity properties to the systems.[1,2,6-12] A necessary first step in understanding the functional behavior of these complicated assemblies is the characterization of the general electronic properties of strongly interacting porphyrinic species.[10,14-18] In this regard, we previously reported an investigation of $\pi\pi$ interactions in the lanthanide porphyrin sandwich complexes, Ce^{IV}-$(OEP)_2$ and $Ce^{IV}(TPP)_2$ (OEP = octaethylporphyrin; TPP = tetraphenylporphyrin), as well as their corresponding π cation radicals.[19] These complexes are of particular interest because

(1) Okamura, M. Y.; Feher, G.; Nelson, N. In *Photosynthesis: Energy Conversion by Plants and Bacteria*; Academic Press: New York, 1982; Vol. 1, pp 195–272.

(2) Hoffman, B. M.; Ibers, J. A. *Acc. Chem. Res.* **1983**, *16*, 15–21, and references therein.

(3) (a) Diesenhofer, J.; Epp, O.; Miki, K.; Huber, R.; Michel, H. *J. Mol. Biol.* **1984**, *180*, 385–398. (b) Diesenhofer, J.; Epp, O.; Miki, K.; Huber, R.; Michel, H. *Nature* **1985**, *318*, 618–624.

(4) Chang, C.-H.; Tiede, D.; Tang, J.; Smith, U.; Norris, J.; Shiffer, M. *FEBS Lett.* **1986**, *205*, 82–86.

(5) Allen, J. P.; Feher, G.; Yeates, T. O.; Komiya, H.; Rees, D. C. *Proc. Natl. Acad. Sci. U.S.A.* **1987**, *84*, 5730–5734.

(6) (a) Martinsen, J.; Stanton, J. L.; Greene, R. L.; Tanaka, J.; Hoffman, B. M.; Ibers, J. A. *J. Am. Chem. Soc.* **1985**, *107*, 6915–6920. (b) Ogawa, M. Y.; Martinsen, J.; Palmer, S. M.; Stanton, J. L.; Tanaka, J.; Green, R. L.; Hoffman, B. M.; Ibers, J. A. *Ibid.* **1987**, *109*, 1115–1121.

(7) Turek, P.; Petit, P.; André, J.-J.; Simon, J.; Even, R.; Boudjema, B.; Guillaud, G.; Maitrot, M. *J. Am. Chem. Soc.* **1987**, *109*, 5119–5122.

(8) Nohr, R. S.; Kuznesof, P. M.; Wynne, K. J.; Kenney, M. E.; Siebenman, P. G. *J. Am. Chem. Soc.* **1981**, *103*, 4371–4377.

(9) Diel, B. N.; Inabe, T.; Lyding, J. W.; Schoch, K. F., Jr.; Kannewurf, C. R.; Marks, T. J. *J. Am. Chem. Soc.* **1983**, *105*, 1551–1567.

(10) Pietro, W. J.; Marks, T. J.; Ratner, M. A. *J. Am. Chem. Soc.* **1985**, *107*, 5387–5391.

(11) Diel, B. N.; Inabe, T.; Taggi, N. K.; Lyding, J. W.; Schneider, O.; Hanack, M.; Kannewurf, C. R.; Marks, T. J.; Schwartz, L. H. *J. Am. Chem. Soc.* **1984**, *106*, 3207–3214.

(12) Collman, J. P.; McDevitt, J. T.; Leidner, C. R.; Yee, G. T.; Torrance, J. B.; Little, W. A. *J. Am. Chem. Soc.* **1987**, *109*, 4606–4614.

(13) Hale, P. D.; Pietro, W. J.; Ratner, M. A.; Ellis, D. E.; Marks, T. J. *J. Am. Chem. Soc.* **1987**, *109*, 5943–5947.

(14) Gouterman, M.; Holten, D.; Lieberman, E. *Chem. Phys.* **1977**, *25*, 139–153.

(15) Hunter, C. A.; Sanders, J. K. M.; Stone, A. J. *Chem. Phys.* **1989**, *133*, 395–404.

(16) Schick, G. A.; Schreiman, I. C.; Wagner, R. W.; Lindsey, J. S.; Bocian, D. F. *J. Am. Chem. Soc.* **1989**, *111*, 1344–1350.

(17) Osuka, A.; Maruyama, K. *J. Am. Chem. Soc.* **1988**, *110*, 4454–4456.

(18) (a) Yan, X.; Holten, D. *J. Phys. Chem.* **1988**, *92*, 409–414. (b) Bilsel, O.; Rodriguez, J.; Holten, D. *J. Phys. Chem.* Submitted for publication.

(19) Donohoe, R. J.; Duchowski, J. K.; Bocian, D. F. *J. Am. Chem. Soc.* **1988**, *110*, 6119–6124.

the two macrocycles are in extremely close proximity.[20] Crystallographic studies of $Ce^{IV}(OEP)_2$ show that the core atoms of the two π macrocycles are on average separated by 3.4 Å, while the distance between the planes defined by the pyrrole nitrogen atoms is only 2.7 Å.[20d] Our spectroscopic studies of the cationic species indicate that the strong $\pi\pi$ interaction leads to delocalization of the hole on the vibrational and electronic time scales.

The ionic radius of Ce^{IV} is among the smallest of the lanthanides;[21] therefore, the magnitude of the $\pi\pi$ interaction and extent of electron delocalization in $Ce^{IV}(OEP)_2^+$ and $Ce^{IV}(TPP)_2^+$ might be expected to be among the largest in the family of lanthanide porphyrin sandwich complexes. To the extent that the interring separation is proportional to the radius of the central metal ion, it should be possible to alter the electronic properties by changing the lanthanide ion. Such an approach has been taken by Buchler and co-workers who have established the methodology for synthesizing all of the $Ln^{III}(OEP)_2$ complexes.[20b,e,f] These systems contain a single hole in the porphyrin π system and are electronically similar to $Ce^{IV}(OEP)_2^+$. Buchler and co-workers have shown that the oxidation potentials of the Ln^{III} sandwiches shift monotonically with the radius of the central metal ion.[20f] A more noteworthy characteristic of the single-hole species is a near-infrared (NIR) absorption band whose wavelength maximum also appears to vary systematically with the radius of the lanthanide ion.[20f] The NIR band was originally viewed as arising from the equivalent of an intervalance charge-transfer transition; however, our recent studies on $Ce^{IV}(OEP)_2^+$ and $Ce^{IV}(TPP)_2^+$ suggest this description is not the most appropriate.[19] Accordingly, a detailed investigation of the NIR spectra of a series of single-hole complexes should provide additional insight into the origin of the NIR absorption.

In this paper, we report absorption and resonance Raman (RR) spectra of a series of $Ln^{III}(OEP)_2$ (Ln = Eu, Nd, La) complexes and compare these data with those obtained for $Ce^{IV}(OEP)_2^+$. The size of these Ln^{III} ions increases successively from 107 (Eu) to 112 (Nd) to 118 pm (La).[21] Crystallographic studies of $Eu^{III}(OEP)_2$ indicate that the separation between the average planes of the porphyrin macrocycles is comparable to that which occurs in $Ce^{IV}(OEP)_2$.[20d,e] We also examine the NIR bands of all four single-hole complexes as a function of temperature and perform a detailed vibronic analysis of the band contours. On the basis of these analyses, we characterize the vibronic coupling and assess the contribution of $\pi\pi$ overlap to intradimer bonding. Collectively, these studies provide a detailed description of the nature of the $\pi\pi$ interaction and the mechanism of hole delocalization in the porphyrin sandwich complexes.

II. Methods

A. Experimental Procedures. The $Ln(OEP)_2$ complexes (Ln = Ce^{IV}, Eu^{III}, Nd^{III}, La^{III}) were prepared by refluxing H_2OEP (Midcentury) and the appropriate $Ln^{III}(acetylacetonate)_3 \cdot xH_2O$ (Alfa, 99.9+% rare earth oxide) in 1,2,4-trichlorobenzene (Aldrich, 99+%) under an inert atmosphere.[20b,d,e] Oxidation of $Ce^{IV}(OEP)_2$ was carried out with phenoxathiinylium hexachloroantimonate in 1,2-dichloroethane (Aldrich, 99+%) under an inert atmosphere.[20c,22] Purification of all the complexes was performed according to the procedures of Buchler et al.[20b-e]

Absorption spectra were collected on a Perkin-Elmer 330 grating spectrophotometer. Routine room-temperature spectra were obtained by using dichloromethane (Fischer Optima Grade) as the solvent. The samples used for room temperature NIR absorption studies were typically prepared to give an optical density (OD) of 1.0 at the maximum of the NIR band. However, the sample concentrations were varied such that

the OD of this band ranged from 0.1 to 3 in order to ascertain whether this influenced the spectral features.

Variable-temperature absorption spectra were obtained with the aid of an APD Cryogenics DE-202 Displex closed-cycle refrigeration system. Initially, the samples used in these studies were prepared in protonated solvents. However, it was found that the large solvent OD in the NIR region (CH combinations and overtones) in concert with a large sample OD resulted in an unacceptable degree of solvent subtraction. This resulted in a loss of spectral resolution in the NIR region. Consequently, all samples used in the variable-temperature studies were prepared in either methylcyclohexane-d_{14} or a 1:1 mixture of dichloromethane-d_2 and toluene-d_8 (all solvents Aldrich, 99+% atom-d). Frozen solution spectra of $Ce^{IV}(OEP)_2^+$ were obtained only in the latter solvent mixture due to solubility. It was also found that the typical scan speed of 480 nm/min resulted in a serious degradation of the spectral resolution in the NIR region. Consequently, all variable-temperature spectra were obtained at a scan speed of 120 nm/min. For all the NIR spectra, the spectral resolution was approximately 50 cm^{-1}.

In order to obtain high quality NIR spectra as the temperature was lowered, it was necessary to decrease successively the sample concentration from that used at room temperature. This compensated for solvent contraction, line narrowing, and Boltzmann effects. Typically, a 10-fold dilution of the room-temperature sample (OD 1.0 at the NIR band maximum) was required to yield a similar OD at 10 K. The trial and error aspect of finding an optimal dilution allowed a de facto investigation of the effect of concentration on the spectral features at different temperatures.

Resonance Raman (RR) spectra were acquired by using instrumentation described elsewhere.[23] The samples were suspended in compressed pellets with a supporting medium of Na_2SO_4 (1:10 ratio). For all the complexes, the incident laser power was approximately 35 mW, and the spectral slit width was approximately 3 cm^{-1}.

B. NIR Band Simulations. The vibronic analysis was performed on an IBM/PC AT computer equipped with a MathCoprocessor. A one-dimensional harmonic Franck–Condon approximation was found to reproduce adequately the observed spectral features (vida infra). In this approximation, the intensity of an individual member of the vibronic progression is given by

$$I_{mn} = M_{ge}^2 |\langle FC \rangle_{mn}|^2 (\nu_{\infty} + m\nu_e - n\nu_g) \exp(-nh\nu_g/kT)/ \\ \sum_n \exp(-nh\nu_g/kT) \quad (1)$$

where M_{ge} is the electronic transition moment and FC are the Franck–Condon overlaps given by the Manneback recursion relations[24]

$$\langle 0|0 \rangle = (a)^{1/2}\exp[-\Delta^2/2(1 + R)] \quad (2)$$

$$\langle m + 1|n \rangle = -b[m/(m + 1)]^{1/2}\langle m - 1|n \rangle + \\ a[n/(m + 1)]^{1/2}\langle m|n - 1 \rangle - c(m + 1)^{-1/2}\langle m|n \rangle \quad (3)$$

$$\langle m|n + 1 \rangle = b[n/(n + 1)]^{1/2}\langle m|n - 1 \rangle + \\ a[m/(n + 1)]^{1/2}\langle m - 1|n \rangle + d(n + 1)^{-1/2}\langle m|n \rangle \quad (4)$$

where

$$R = \nu_g/\nu_e \quad (5)$$

$$a = (R - 1)/(R + 1) \quad (6)$$

$$b = 2R^{1/2}/(R + 1) \quad (7)$$

$$c = \Delta(2R)^{1/2}/(R + 1) \quad (8)$$

$$d = 2^{1/2}\Delta/(R + 1) \quad (9)$$

Here n and m are the vibrational quanta in the ground and excited electronic states; ν_g and ν_e are the vibrational frequencies in these two states; ν_{∞} is the frequency of the electronic transition; Δ is the origin shift expressed in the ground-state dimensionless coordinate.

III. Results

A. Absorption Spectra. The room-temperature absorption spectra of $Eu^{III}(OEP)_2$, $Nd^{III}(OEP)_2$, and $La^{III}(OEP)_2$ are compared with those of $Ce^{IV}(OEP)_2^+$ and $Ce^{IV}(OEP)_2$ in Figure 1. The spectra of all three neutral $Ln^{III}(OEP)_2$ complexes exhibit broad Soret and low intensity Q bands. These features are atypical of neutral porphyrins (Figure 1a) but are typical of porphyrin π cation radicals (Figure 1b).[25] The similarity of the general

(20) (a) Buchler, J. W.; Kapellmann, H.-G.; Knoff, M.; Lay, K.-L.; Pfeifer, S. *Z. Naturforsch. B, Anorg. Chem., Org. Chem.* **1983**, *38B*, 1339–1345. (b) Buchler, J. W.; Knoff, M. In *Optical Properties and Structure of Tetrapyrroles*; Blauer, G., Sund, H., Eds.; de Gruyter: West Berlin, 1985; pp 91–105. (c) Buchler, J. W.; Elsässer, K.; Kihn-Botulinski, M.; Scharbert, B. *Angew. Chem., Int. Ed. Engl.* **1986**, *25*, 286–287. (d) Buchler, J. W.; DeCian, A.; Fischer, J.; Kihn-Botulinski, M.; Paulus, H.; Weiss, R. *J. Am. Chem. Soc.* **1986**, *108*, 3652–3659. (e) Buchler, J. W.; de Cian, A.; Fischer, J.; Kihn-Botulinski, M.; Weiss, R. *Inorg. Chem.* **1988**, *27*, 339–345. (f) Buchler, J. W.; Scharbert, B. *J. Am. Chem. Soc.* **1988**, *110*, 4272–4276.

(21) Shannon, R. D.; Prewitt, C. T. *Acta Crystallogr., Sect. B: Struct. Crystallogr. Cryst. Chem.* **1969**, *B25*, 928–929.

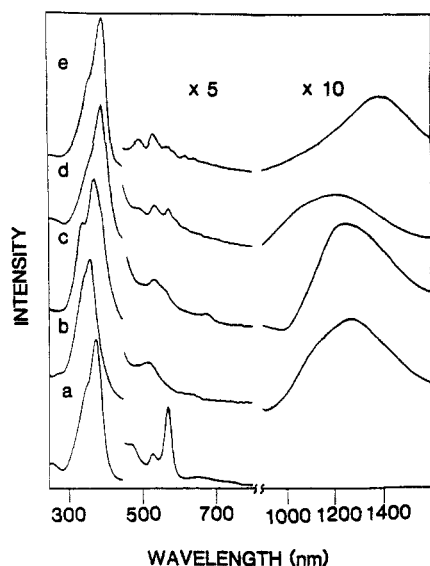(22) Gans, P.; Marchon, J.-C.; Reed, C. A.; Regnard, J.-R. *Nouv. J. Chim.* **1981**, *5*, 203–204.

Figure 1. Room-temperature absorption spectra of (a) $Ce^{IV}(OEP)_2$, (b) $Ce^{IV}(OEP)_2^+$, (c) $Eu^{III}(OEP)_2$, (d) $Nd^{III}(OEP)_2$, and (e) $La^{III}(OEP)_2$ in dichloromethane.
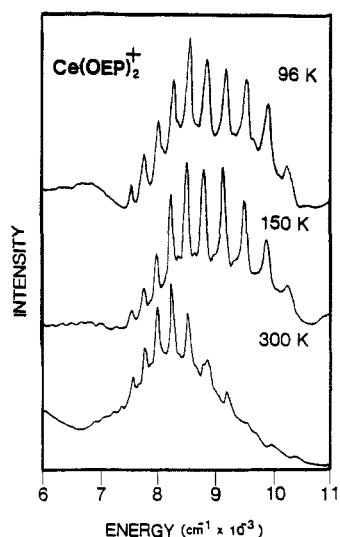
Figure 2. Variable-temperature NIR spectra of $Ce^{IV}(OEP)_2^+$ in dichloromethane-d_2/toluene-d_8 (1:1).

Figure 3. Variable-temperature NIR spectra of $Eu^{III}(OEP)_2$ in methylcyclohexane-d_{14}.
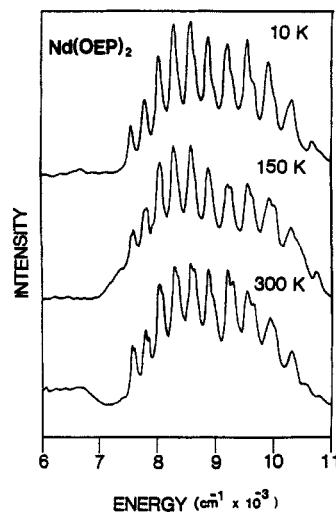
Figure 4. Variable-temperature NIR spectra of $Nd^{III}(OEP)_2$ in methylcyclohexane-d_{14}.

features of the UV-vis spectra of $Ce^{IV}(OEP)_2^+$ and the Ln^{III}-$(OEP)_2$ complexes is indicative of the hole which resides in the π system of the latter species.[20c,f] The presence of a hole in the porphyrin π system of the Ln^{III} double deckers is further confirmed by the appearance of the NIR absorption band. A particularly noteworthy aspect of the absorption spectra of the $Ln^{III}(OEP)_2$ complexes is that they do not appear to be comprised of features associated with separate neutral and oxidized chromophores isolated within a single molecule. This behavior is analogous to that observed for the Ce^{IV} porphyrin cations[19] and suggests that the hole is delocalized in all of the Ln^{III} sandwiches examined, regardless of the size of the ion. In this regard, composite absorption spectra are typically observed in transition-metal complexes wherein the redox orbital is known to be localized on one ligand of a multiligand system.[26-29]
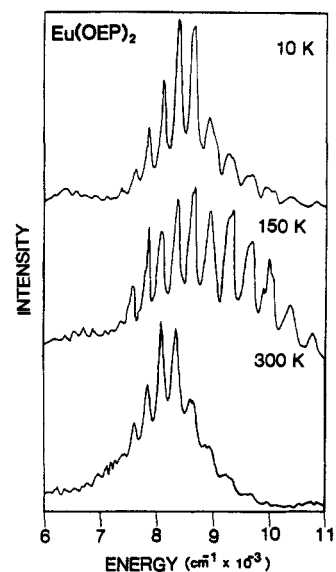
The NIR absorption spectra shown in Figure 1 were recorded in protonated solvents with a scan speed of 480 nm/min. Under these conditions, the NIR bands are broad and featureless and exhibit a general appearance similar to that previously reported.[20c,f] Variable-temperature NIR spectra of the Ce^{IV}, Eu^{III}, Nd^{III}, and La^{III} single-hole complexes are shown in Figures 2, 3, 4, and 5, respectively. These spectra were recored in deuteriated solvents with a scan speed of 120 nm/min. As is evident, the NIR bands of all four complexes exhibit well-resolved fine structure even at room temperature. For $Ce^{IV}(OEP)_2^+$ and $Eu^{III}(OEP)_2$, the room-temperature spectra are dominated by a single, relatively harmonic progression where the spacing between the vibronic components is $\sim$250 cm^{-1} (cf. Figures 2 and 3, bottom). In the case of $Nd^{III}(OEP)_2$ and $La^{III}(OEP)_2$, the room-temperature spectra are more complicated and appear to be comprised of two separate, relatively harmonic progressions. The progression on the low-energy side of the band has a spacing comparable to that observed for $Ce^{IV}(OEP)_2^+$ and $Eu^{III}(OEP)_2$, whereas on the

(23) Donohoe, R. J.; Atamian, M.; Bocian, D. F. *J. Am. Chem. Soc.* **1987**, *109*, 5593–5599.

(24) Manneback, C. *Physica* **1951**, *XVII*, 1001–1010.

(25) Felton, R. H. In *The Porphyrins*; Dolphin, D., Ed.; Academic Press: New York, 1978; Vol. V, pp 53–125.

(26) Edwards, W. D.; Zerner, M. C. *Can. J. Chem.* **1985**, *63*, 1763–1772.

(27) Heath, G. A.; Yellowlees, L. J.; Braterman, P. S. *J. Chem. Soc., Chem. Commun.* **1981**, 287–289.

(28) Elliot, C. M.; Hershenhart, E. *J. Am. Chem. Soc.* **1982**, *104*, 7519–7526.

(29) (a) Angel, S. M.; DeArmond, M. K.; Donohoe, R. J.; Wertz, D. W. *J. Phys. Chem.* **1985**, *89*, 282–285. (b) Donohoe, R. J.; Tait, C. D.; DeArmond, M. K.; Wertz, D. W. *Spectrochim. Acta* **1986**, *42A*, 233–240. (c) Tait, C. D.; MacQueen, D. B.; Donohoe, R. J.; DeArmond, M. K.; Hanck, K. W.; Wertz, D. W. *J. Phys. Chem.* **1986**, *90*, 1766–1771. (d) Donohoe, R. J.; Tait, C. D.; DeArmond, M. K.; Wertz, D. W. *Ibid.* **1986**, *90*, 3923–3926. (e) Donohoe, R. J.; Tait, C. D.; DeArmond, M. K.; Wertz, D. W. *Ibid.* **1986**, *90*, 3927–3930.
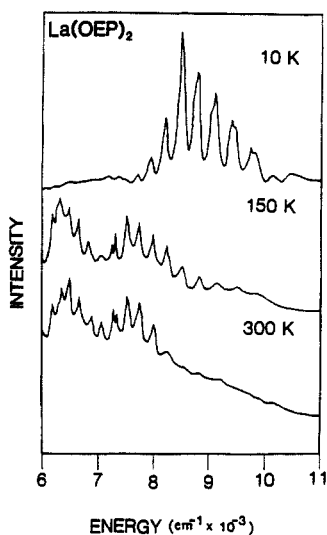
Figure 5. Variable-temperature NIR spectra of $La^{III}(OEP)_2$ in methylcyclohexane-d_{14}.

high-energy side, the spacing is ~ 315 cm^{-1} (cf. Figures 4 and 5, bottom). When the temperature is lowered to 150 K, a second progression with a spacing of ~ 315 cm^{-1} is also observed on the high-energy side of the NIR bands of $Ce^{IV}(OEP)_2{}^+$ and Eu^{III}-$(OEP)_2$ (cf. Figures 2 and 3, middle). This progression grows monotonically as the temperature is lowered from 300 to 150 K. [Closer inspection of the 300 K NIR spectra of $Ce^{IV}(OEP)_2{}^+$ and $Eu^{III}(OEP)_2$ reveals that the second progression is also present at room temperature.] At 150 K, both progressions are still clearly present in the NIR spectra of both $Nd^{III}(OEP)_2$ and $La^{III}(OEP)_2$ (cf. Figures 4 and 5, middle). In the case of the latter complex, it appears that the third progression could also be present at somewhat higher energy (ca. 8000–9000 cm^{-1}). At the lowest temperatures at which NIR spectra were recorded (10 K for the three $Ln^{III}(OEP)_2$ complexes and 96 K for $Ce(OEP)_2{}^+$; spectra were not obtainable below 96 K for the latter complex due to cracking of the solvent glass), the two progressions are observed in the spectra of all the complexes (cf. Figures 2–5, top). Interestingly, the relative contribution of the progression on the high-energy side of the NIR band of $Eu(OEP)_2$ is less than that observed at 150 K. The contribution of this progression appears to be maximum in the range 100–150 K and declines monotonically as the temperature is lowered below 100 K. In addition, the two progressions observed for $La(OEP)_2$ are now centered at approximately the same energy as those observed for the other three complexes. These two progressions appear to grow in as the temperature is lowered below 100 K. It is not clear whether they are new (perhaps the third progression in the 150 K spectrum) or are the same progressions observed at 300 and 150 K except shifted to higher energy. Examination of the NIR spectrum at several intermediate temperatures (not shown) does not resolve this issue.

Several other experiments were performed in attempts to characterize further the nature of the two vibronic progressions observed in the NIR region. First, the temperature was cycled in order to determine whether this influenced the relative contribution of the two progressions at a given temperature. In all cases, no annealing effects were observed, and the spectra appear to be identical with those shown in the figures. Next, the effect of changing the type of solvent and/or the sample concentration was explored. Again, this appeared to have no effect on the relative contribution of the two progressions to the band contours of any of the complexes at any temperature. Finally, the UV–vis regions of the absorption spectra were examined over a range of temperatures where the two progressions make widely disparate contributions to the total NIR band intensity. Regardless of the nature of the NIR profile, the low-temperature UV–vis spectra are essentially identical with those observed at room temperature (Figure 1) except for a small amount of line narrowing.
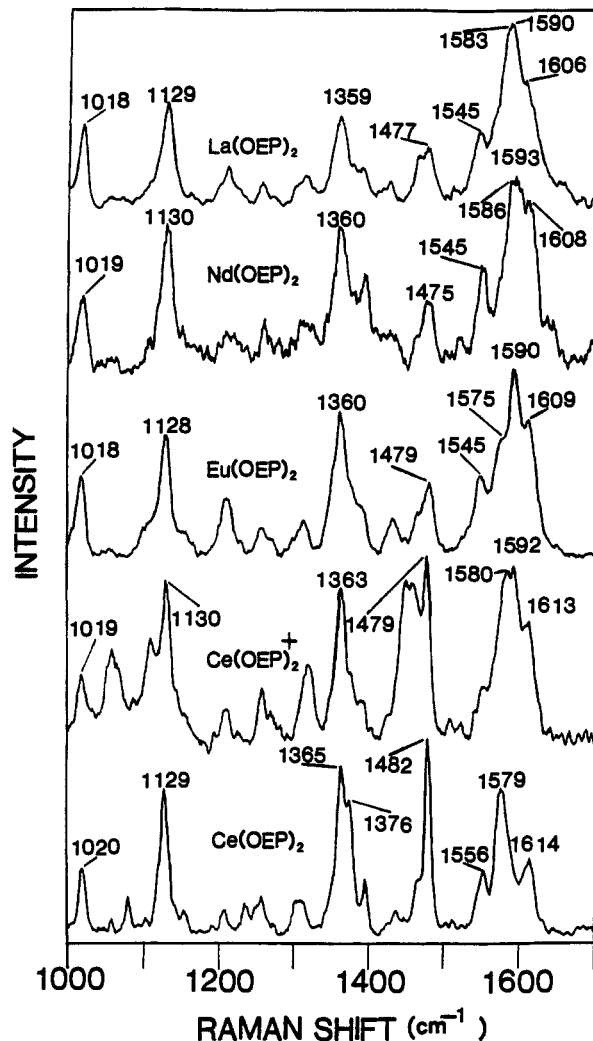

Figure 6. High-frequency regions of the B state excitation ($\lambda_{ex} = 363.8$ nm) RR spectra of the $Ln(OEP)_2$ complexes in Na_2SO_4 pellets.

Table I. Resonance Raman Frequencies (cm^{-1}) of the $Ln(OEP)_2$ Complexes

	$Ce(OEP)_2$	$Ce(OEP)_2{}^+$	$Eu(OEP)_2$	$Nd(OEP)_2$	$La(OEP)_2$
ν_2	1579	1592	1590	1591	1593
ν_3	1482	1479	1479	1475	1477
ν_4	1376	1363	1360	1360	1359
ν_{10}	1614	1613	1609	1608	1606
ν_{11}	1556	1580	1575	1586	1583

B. RR Spectra. The high-frequency regions of the B-state excitation ($\lambda_{ex} = 363.8$ nm) RR spectra of $Eu^{III}(OEP)_2$, Nd^{III}-$(OEP)_2$, and $La^{III}(OEP)_2$ are compared with those of $Ce^{IV}(OEP)_2{}^+$ and $Ce^{IV}(OEP)_2$ in Figure 6. RR spectra were also obtained at a number of other excitation wavelengths throughout the violet-blue and yellow-green regions of the absorption spectra (not shown). The frequencies of selected vibrational modes are summarized in Table I. The general features of the band envelopes in the 1550–1620-cm^{-1} regions of the spectra of the three $Ln^{III}(OEP)_2$ complexes are similar to those observed for Ce^{IV}-$(OEP)_2{}^+$. These features are typical of those observed in the RR spectra when a hole resides in an a_{1u} orbital of the porphyrin ring.[30,31] In particular, the ν_2 and ν_{11} bands of all the single-hole complexes are substantially upshifted relative to those of the neutral $Ce^{IV}(OEP)_2$, whereas the ν_4 bands of the former species are downshifted relative to that of the latter. As is the case for $Ce^{IV}(OEP)_2{}^+$, the RR spectra of the $Ln^{III}(OEP)_2$ complexes are comprised of a single set of peaks. There is no evidence of com-

(30) Oertling, W. A.; Salehi, A.; Chung, Y. C.; Leroi, G. E.; Chang, C. K.; Babcock, G. T. *J. Phys. Chem.* **1987**, *91*, 5887–5898.

Table II. NIR Band Simulation Parameters for $Ln(OEP)_2$ Complexes

compd	$\nu_{00}^{I\,a}$	ν_g^{I}	ν_e^{I}	Δ^{I}	$\delta_r^{I\,b}$	ν_{00}^{II}	ν_g^{II}	ν_e^{II}	Δ^{II}	δ_r^{II}	$c^{I}/c^{II\,c}$
$La(OEP)_2$	7720	370	260	3.00	0.056	8210	440	315	2.85	0.049	1.23
$Nd(OEP)_2$	7545	370	260	2.95	0.055	8295	430	320	2.80	0.049	1.09
$Eu(OEP)_2$	7602	360	250	2.75	0.052	8002	440	310	2.60	0.045	1.59
$Ce(OEP)_2^{+}$	7528	360	250	2.70	0.051	8228	445	315	2.60	0.044	1.01^{d}

[a] All frequencies in cm^{-1}. *[b]* δ_r in Å. *[c]* At 10 K. *[d]* At 96 K, see text.

posite features due to one neutral and one fully oxidized porphyrin moiety. Such composite RR spectra are typically observed for systems in which the redox orbital is known to be confined to a portion of the molecular framework.[29,32] Finally, we could find no obvious features in the RR spectra (high or low frequency) of any of the complexes which would indicate that the vibrational frequencies are particularly sensitive to the effect which results in varying contributions of the two vibronic progressions to the NIR band contour. In addition, no atypical RR band(s) is (are) observed in the low-frequency region which can be assigned as the ground-state counterpart(s) of the mode(s) which exhibit vibronic activity in the NIR region.

C. NIR Band Simulations. The general appearance of the NIR bands of the single-hole complexes is that of a complicated contour with at least two vibronically active modes of different frequency. Accordingly, we initially attempted to simulate the NIR bands by using a multidimensional Franck–Condon approximation where the various progressions are built off a single system origin. The first calculations were performed on the spectra obtained at the lowest temperatures (see Figures 2–5, top). In these calculations, the ground-state vibrational frequencies, origin shifts, and the energy of the system origin were allowed to vary. The excited-state vibrational frequencies were fixed by the vibronic spacings observed in the NIR spectra. In all cases, this approach failed. Ultimately, we found that the NIR band contours can only be reproduced if two system origins, separated by 400–700 cm^{-1} (depending on the complex), are present. With use of this approach, the low-temperature NIR spectra can be well accounted for by summing the spectral contours generated by using a one-dimensional Franck–Condon approximation for each vibronic progression. The progression with a spacing of ~250 cm^{-1} is built off the lower energy origin, ν_{00}^{I}, while that with a spacing of ~315 cm^{-1} is built off the higher energy origin, ν_{00}^{II}. The relative contribution of the two progressions to the total band contour can be accounted for by scaling the integrated intensity of one progression with respect to another. The fact that the NIR spectra can be simulated in this manner suggests that (at least) two distinct forms of the complexes are present and that the relative concentrations of the two forms, c^{I}/c^{II}, are temperature dependent.

The set of parameters derived from fitting the 10 K (96 K for $Ce(OEP)_2^{+}$) NIR band contours of the $Ln(OEP)_2$ complexes is given in Table II. The value of c^{I}/c^{II} at this temperature is also indicated in the table. Inspection of Table II reveals several noteworthy features. First, the spectral parameters for the NIR bands of all the complexes are quite similar; only c^{I}/c^{II} differs significantly. Second, the predicted ground-state vibrational frequencies, ν_g, of the Franck–Condon active mode are ~120 cm^{-1} larger than those of the excited state, ν_e, for both forms I and II. Finally, the dimensionless origin shifts Δ, along this coordinate are quite large for both forms, ranging from 2.60 to 3.00. In general, the origin shifts calculated for form I are slightly larger than those calculated for form II.

The 10 K NIR band contours calculated for $Eu(OEP)_2$ and $La(OEP)_2$ by using the parameters given in Table II are compared with the observed spectra in Figures 7 and 8, respectively. The individual contours calculated for forms I and II are also shown in the figure. In the spectral simulations, the electronic transition moments were assumed to be identical for the two forms. The vibronic lines were approximated as gaussians with a full width
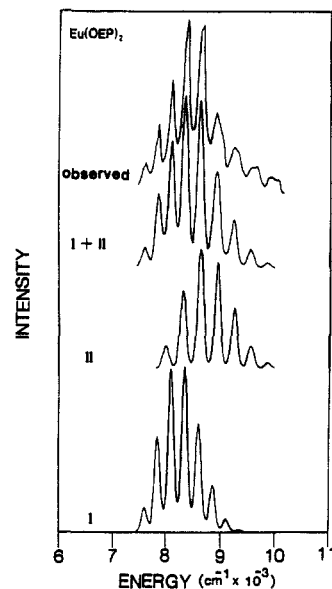

Figure 7. Observed and simulated 10 K NIR spectra of $Eu^{III}(OEP)_2$. The spectra labeled I and II were calculated by using the parameters given in Table II. The relative integrated intensities are scaled to the value of c^{I}/c^{II} given in the table. The total calculated band contour, labeled I + II, is the sum of the two individual contours.

at half maximum of 135 cm^{-1}. During the course of the fitting procedures, a range of ν_{00}, ν_g/ν_e, Δ, and c^{I}/c^{II} values was explored. Altering the relative positions of the system origins of the two conformers from those given in Table II necessitates physically unreasonable values of ν_g/ν_e and Δ. On the other hand, the values of ν_g/ν_e and Δ can be altered by as much as 10% without significantly degrading the quality of the fits.

Excellent fits can be obtained for the higher temperature spectra of all the complexes, with the exception of $La(OEP)_2$, by using the parameters listed in Table II and altering c^{I}/c^{II}. The quality of the fits can be further enhanced if the origin shifts are also allowed to vary a small amount (1–2%) as a function of temperature. The NIR spectra of $La(OEP)_2$ obtained at temperatures above 100 K cannot be fit by using the values of ν_{00} given in Table II because the energies of the system origins appear to change with temperature (see Figure 5). In addition, the intensity of the NIR band of this complex is significantly attenuated at higher temperatures. The resulting relatively low signal-to-noise ratio precludes an accurate simulation of these spectra. Consequently, it is not clear whether the ground-state vibrational frequencies and/or the origin shifts of the vibronically active mode might not also be a function of temperature.

IV. Discussion

A. General Characteristics of the Single-Hole Sandwich Complexes. The general features of the absorption and RR spectra of all the single-hole complexes are consistent with complete delocalization of the hole on the vibrational (10^{-13} s) and electronic time scales (10^{-15} s). The appearance of the NIR band contours is further consistent with delocalization occurring through direct $\pi\pi$ overlap (vide infra). These results indicate that although the size of the central metal ion may mediate the magnitude of the $\pi\pi$ interaction, the separation between the porphyrin π systems is not sufficiently large in any of the complexes to result in a measurable barrier to hole transfer.

One feature of the absorption spectra which remains to be explained is the origin of the multiple progressions observed in

(31) Czernuszewicz, R. S.; Macor, K. A.; Li, X.-Y.; Kincaid, J. R.; Spiro, T. G. *J. Am. Chem. Soc.* **1989**, *111*, 3860–3880.
(32) Angel, S. M.; DeArmond, M. K.; Donohoe, R. J.; Hanck, K. W.; Wertz, D. W. *J. Am. Chem. Soc.* **1984**, *106*, 3688–3689.
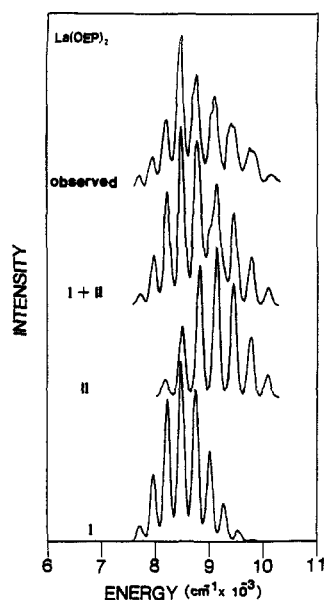
Lanthanide Octaethylporphyrin Sandwich Complexes

J. Am. Chem. Soc., Vol. 112, No. 9, 1990 3317

Figure 8. Observed and simulated 10 K NIR spectra of $La^{III}(OEP)_2$. The spectra labeled I and II were calculated by using the parameters given in Table II. The relative integrated intensities are scaled to the value of c^I/c^{II} given in the table. The total calculated band contour, labeled I + II, is the sum of the two individual contours.

Figure 9. Partial molecular orbital diagram for the single-hole porphyrin sandwich complexes. The intradimer charge-transfer transition which gives rise to the NIR absorption involves promotion of an electron from the b_1 to the a_2 molecular orbital and is labeled accordingly.

the NIR region. As indicated is section IIIC, the temperature dependence of the relative contributions of the two progressions to the band contours suggests that two different forms of the complexes are present. The RR and UV–vis spectra are apparently insensitive to their presence. One possible explanation is that the two forms differ in the orientation of the ethyl substituent groups with respect to the porphyrin planes. In this regard, monomeric $Ni^{II}OEP$ is known to crystallize in at least three distinct forms all of which exhibit different conformations of the ethyl substituents.[33-35] Different orientations of the ethyl groups could give rise to different steric interactions between the macrocycles. This in turn could alter the magnitude of the $\pi\pi$ overlap and affect the spectral parameters associated with the NIR absorption band. Furthermore, altering the orientation of the ethyl groups would not be expected to affect the UV–vis spectra or to a large extent the RR spectra.[35]

Inasmuch as there are hundreds of possible conformations of the 16 ethyl substituents in the sandwiches, certain orientations must be strongly preferred to produce only two principal NIR absorption bands. However, the line widths of the vibronic transitions are quite large even at 10 K ($\sim$135 cm^{-1}). It is possible that the heterogenous widths associated with these lines arise from unresolved NIR transitions from a large number of conformers in which the steric constraints and $\pi\pi$ interactions are similar. The unusual temperature dependence observed for the NIR band of La(OEP)$_2$ (see Figure 5) can also be rationalized in terms of multiple conformations. As the distance between the planes of the macrocycles increases, the steric constraints should be attenuated. Accordingly, the ethyl groups of this complex might be more free to rotate or assume less preferred orientations at higher temperatures than those of the more sterically hindered complexes. Regardless, at very low temperatures, all the complexes appear to adopt the same two principal conformations. In attempts to gain a more detailed understanding of the structural features which give rise to the two principal forms, we are examining NIR spectra of single-hole complexes prepared from porphyrins with other types of substituent groups and/or with substituent groups located at different positions on the macrocycle.
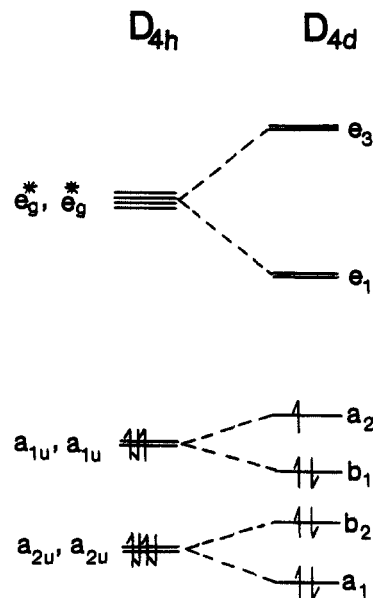
B. Nature of the Vibronic Interactions. The general appearance of the NIR band contours of the single-hole sandwich complexes can be explained in terms of the theoretical models which have been developed for mixed-valence line shapes.[36-38] In this regard, Piepho[38] has recently modified the original Piepho, Krausz, and Shatz (PKS) vibronic model[36] such that the effects of strong overlap can be included explicitly. In this new model, the zero-order electronic wave functions are taken to be molecular orbitals formed from linear combinations of the highest occupied molecular orbitals of the monomer units which comprise the dimer. This is illustrated for the single-hole sandwich complexes in the partial molecular orbital diagram shown in Figure 9. In the figure, the porphyrin orbitals are shown in the limits of zero (left side) and strong (right side) porphyrin–porphyrin interaction. The orbitals of the constituent monomers are energetically ordered in a fashion appropriate for OEP and labeled according to D_{4h} symmetry.[39] The dimer orbitals are labeled according to D_{4d} symmetry which is the approximate symmetry of Ce(OEP)$_2$ and Eu(OEP)$_2$.[20d,e] The exact energies and splittings of the molecular orbitals derived from the a_{1u} and a_{2u} monomer orbitals are not known and have been ordered for pictorial clarity. The hole is, however, in an a_{1u}-derived dimer molecular orbital (see section IIIB). In this orbital scheme, promotion of an electron from the filled b_1 (bonding) to the half-filled a_2 (antibonding) orbital represents a z-polarized, allowed intradimer charge-transfer transition whose energy is determined, in part, by the extent of overlap. This transition results in the NIR absorption feature.[19]

In the Piepho model in lowest level of approximation, three types of vibrational modes can give rise to vibronic structure on the intradimer charge-transfer band.[38] Two of these are derived from linear combinations of modes which are present in the constituent monomers before dimerization. The third mode is a multicenter vibration which is only present in the dimer. Vibronic coupling through the third mode is a feature which appears as a result of overlap and is not accounted for in the PKS model.[36] In the sandwich porphyrins, linear combinations of A_{2u} (D_{4h} symmetry) out-of-plane deformations of the monomeric units are of the appropriate symmetry to gain vibronic activity in the intradimer charge-transfer transition. A symmetric linear combination of such modes, Q_+, yields an A_{1g} (A_1 in D_{4d} symmetry) Franck–Condon active dimer vibration, while an antisymmetric linear combination, Q_-, results in an A_{2u} (B_2 in D_{4d} symmetry) pseu-

(33) Meyer, E. F., Jr. *Acta Crystallogr., Sect. B: Struct. Crystallogr. Cryst. Chem.* **1972**, *B28*, 2162–2167.

(34) Cullen, D. L.; Myer, E. F., Jr. *J. Am. Chem. Soc.* **1974**, *96*, 2095–2102.

(35) Brennan, R. D.; Scheidt, W. R.; Shelnutt, J. A. *J. Am. Chem. Soc.* **1988**, *110*, 3919–3924.

(36) Piepho, S. B.; Krausz, E. R.; Schatz, P. N. *J. Am. Chem. Soc.* **1978**, *100*, 2996–3005.

do-Jahn–Teller active mode which couples the two zero-order electronic states. The multicenter mode, Q_{AB}, in the sandwich complexes can be viewed as a Franck-Condon active A_{1g} (A_1 in D_{4d}) pure dimer vibration that modulates the interring separation.

In systems which are partially delocalized, such as type II mixed-valence complexes,[40] Q_- is expected to be the dominant contributor to the vibronic band contour.[38] These bands are characterized by asymmetric shapes and anharmonic progressions. In contrast, when strong overlap and substantial delocalization occurs, Q_{AB} is expected to make an important contribution to the band contour.[38] In a completely delocalized system this mode is expected to dominate. [The Q_+ modes can also contribute to the band contour in the strong overlap limit.] Under these circumstances, the vibronic model reduces to the case of a displaced oscillator. The band shape is highly symmetrical and exhibits fairly regularly spaced peaks (depending on the degree of intrinsic anharmonicity). The NIR band contours observed for the single-hole sandwich complexes clearly resemble the latter case (neglecting the presence of multiple conformers). In fact, there is no evidence of any significant underlying vibronic structure which would be indicative of contributions by Q_-. It should be noted that the vibronically active mode in the sandwich dimers is most likely a linear combination of the pure multicenter vibration and certain Q_+ modes. The relatively high frequency suggests that there could be some pyrrole tilting and/or metal–nitrogen stretching character. Regardless, in the limit of complete delocalization, the concept of intervalence charge transfer is not meaningful because both centers possess the same valence in the ground and excited electronic states. Promotion of the electron only redistributes charge density from between the two macrocycles (the large overlap region) to the top and bottom of the sandwich (the zero-overlap region).

C. Contribution of $\pi\pi$ Interaction to Intradimer Bonding. The spectroscopic data compiled in Table II can be used to assess the contribution of $\pi\pi$ interaction to the intradimer bonding in the ground electronic state of the sandwich complexes. In this state, there is net bonding interaction between the π clouds of the two porphyrinic macrocycles (a multicenter σ bond resulting from π overlap) because the bonding (b_1) orbital is doubly occupied, whereas the antibonding orbital (a_2) is singly occupied. Promotion of an electron from the b_1 to a_2 orbital (the NIR transition) results in an excited electronic state with net antibonding character between the π clouds of the macrocycles. The difference in bond order between the ground and excited states should be manifested both in the equilibrium interring separation and in the force constants for the Q_{AB} mode.

The Δ's obtained from the spectral simulations can be used to estimate the difference in interring separation between the ground and excited electronic states. If the Q_{AB} vibration is approximated as a two-body motion of reduced mass, μ (half the mass of one of the porphyrin rings, $\mu = 266$ AMU), the Cartesian displacement, δ_r, can be obtained from the transformation[41,42]

$$\delta_r = \Delta/0.17(\mu\nu_g)^{1/2} \qquad (10)$$

where δ_r is in Å, μ is in AMU, and ν_g is in cm^{-1}. The values of δ_r obtained for the various complexes are given in Table II. [The interring separation is presumed to be larger in the excited state than in the ground state due to the absence of $\pi\pi$ overlap bond order in the former state.] As can be seen, δ_r is approximately 0.05 Å for all the complexes. The δ_r's for the two conformers are comparable although those of form I appear to be slightly larger than those of form II.

A second measure of the contribution of $\pi\pi$ overlap to intradimer bonding can be obtained by comparing ν_g and ν_e. The

potential energy associated with the Q_{AB} vibration in the ground electronic state arises from two sources, the linkage between the porphyrins via the central metal ion and the linkage via direct $\pi\pi$ interaction. In the excited electronic state, only the linkage via the metal ion can contribute to the harmonic component of the potential energy of the Q_{AB} mode. To a first approximation, this contribution should be similar to that in the ground state because in either state the electrons occupy orbitals derived from a_{1u} porphyrinic orbitals. The antibonding interaction between the π clouds will contribute only to the anharmonic terms in the excited-state potential function because this interaction is purely repulsive. Inasmuch as the vibronic progressions observed in the NIR spectra are quite harmonic, the $\pi\pi$ antibonding interaction must make a negligible contribution to the excited-state potential of the Q_{AB} mode. Accordingly, the difference between ν_g and ν_e can be viewed as an approximate measure of the contribution of $\pi\pi$ interaction to intradimer bonding in the ground electronic state.

Inspection of Table II reveals that the differences between ν_g and ν_e are ~120 cm^{-1} for either form of all the sandwich complexes. Thus, $\pi\pi$ overlap is estimated to represent on the order of 1/3 (form I) to 1/4 (form II) of the total intradimer bonding in the ground state. In general, the differences between ν_g and ν_e are slightly larger for form II (by ~10 cm^{-1}) which suggests a slightly larger $\pi\pi$ overlap. The fact that ν_{00}^{II} is greater than ν_{00}^{I} is also consistent with a somewhat larger $\pi\pi$ interaction in the former conformer. Inasmuch as ν_e^{II} is larger than ν_e^{I}, it appears that the linkage via the central metal ion is also stronger in form II. It seems reasonable that steric contraints would affect the structural feature as well as the extent of $\pi\pi$ overlap.

D. Comparison with the Special Pair in Bacterial Photosynthetic Reaction Centers. It is interesting to compare the intradimer interactions in the sandwich complexes with those which might be expected to occur between the bacteriochlorophyll molecules which comprise the special pair in the bacterial photosynthetic reaction centers. In the protein system, the interring separation (~3.4 Å) is comparable to that in the sandwich complexes; however, the macrocycles are not covalently linked and are not cofacial.[3–5] Consequently, the extent of $\pi\pi$ interaction should be less than that which occurs in the sandwiches. Nevertheless, oxidation of the special pair results in the appearance of a NIR absorption band ca. 1300 nm.[43–45] To the extent that this band is of similar origin to that observed for the sandwich complexes, a vibration that modulates interring separation should contribute to the vibronic band contour. In the special pair dimer, the forces between the bacteriochlorophyll molecules and the protein matrix as well as the $\pi\pi$ overlap should contribute to the frequency of the intradimer mode. These relatively weak forces should result in a lower frequency for Q_{AB} in the special pair than in the sandwich complexes. In this regard, it has been suggested that a 100 cm^{-1} intradimer phonon mode plays an important role in the initial steps of light-activated charge separation.[46] [It should be noted that this mode is characteristic of the neutral special pair dimer. The $\pi\pi^*$ excited state of a neutral dimer in the strong overlap limit would more closely resemble the ground electronic state of a two-hole complex.] It would be interesting to examine the NIR bands of the oxidized special pair dimer at high resolution and/or low temperature in order to determine the detailed shape of the band contour and gain an estimate of the extent of hole delocalization. We are currently in the process of performing such an investigation on the reaction center protein from *Rhodobacter sphaeroides*.

(37) Wong, K. Y.; Schatz, P. N. *Prog. Inorg. Chem.* **1981**, *28*, 369–449.

(38) Piepho, S. B. *J. Am. Chem. Soc.* **1988**, *110*, 6319–6326.

(39) Gouterman, M. In *The Porphyrins*; Dolphin, D., Ed.; Academic Press: New York, 1978; Vol. III, pp 1–165.

(40) Robin, M. B.; Day, P. *Adv. Inorg. Chem. Radiochem.* **1967**, *10*, 247–422.

(41) Peticolas, W. W.; Blazej, D. C. *Chem. Phys. Lett.* **1979**, *63*, 604–608.

(42) Schick, G. A.; Bocian, D. F. *J. Am. Chem. Soc.* **1984**, *106*, 1682–1694.

(43) Dutton, P. L.; Kauffmann, K. J.; Chance, B.; Rentzepis, P. M. *FEBS Lett.* **1975**, *60*, 275–280.

(44) Fajer, J.; Burne, D. C.; Davis, M. S.; Forman, A.; Spaulding, L. D. *Proc. Natl. Acad. Sci. U.S.A.* **1975**, *72*, 4956–4960.

(45) Davis, M. S.; Forman, A.; Hanson, L. K.; Thornber, J. P.; Fajer, J. *J. Phys. Chem.* **1979**, 3325–3332.

(46) Warshel, A. *Proc. Natl. Acad. Sci. U.S.A.* **1980**, *77*, 3105–3109.